Theory of inelastic light scattering in spin-1 systems: Resonant regimes and detection of quadrupolar order

F. Michaud,[1] F. Vernay,[2] and F. Mila[1]

[1]*Institute of Theoretical Physics, Ecole Polytechnique Fédérale de Lausanne, CH-1015 Lausanne, Switzerland*

[2]*Laboratoire PROMES (UPR-8521) & UPVD, Perpignan, France*

(Received 18 August 2011; revised manuscript received 25 October 2011; published 16 November 2011)

Motivated by the lack of an obvious spectroscopic probe to investigate nonconventional order such as quadrupolar orders in spin $S > \frac{1}{2}$ systems, we present a theoretical approach to inelastic light scattering for spin-1 quantum magnets in the context of a two-band Hubbard model. In contrast to the $S = \frac{1}{2}$ case, where the only type of local excited state is a doubly occupied state of energy U, several local excited states with occupation up to four electrons are present. As a consequence, we show that two distinct resonating scattering regimes can be accessed depending on the incident photon energy. For $\hbar\omega_{\rm in} \lesssim U$, the standard Loudon-Fleury operator remains the leading term of the expansion as in the spin-$\frac{1}{2}$ case. For $\hbar\omega_{\rm in} \lesssim 4U$, a second resonant regime is found with a leading term that takes the form of a biquadratic coupling $\sim(\mathbf{S}_i \cdot \mathbf{S}_j)^2$. Consequences for the Raman spectra of $S = 1$ magnets with magnetic or quadrupolar order are discussed. Raman scattering appears to be a powerful probe of quadrupolar order.

DOI: 10.1103/PhysRevB.84.184424 PACS number(s): 78.30.Am, 75.10.Jm, 75.10.Lp

I. INTRODUCTION

The theoretical quest for exotic phases of magnetic matter over the past few decades has opened the way for a systematic investigation of models by various analytical and numerical means and has led to the conceptual understanding of different states. This is, for instance, the case of resonating valence bond states, which have been investigated in the context of high-T_c superconductors,[1] frustrated spin systems,[2] and quantum dimer models.[3,4] Yet, suggesting a technique to unravel the experimental fingerprints of an exotic phase often remains a challenge: for instance, in the spin liquid case, it is only recently that theoretical proposals have been made to detect this state on the kagome lattice with Raman scattering[5,6] and that experiments have been carried out.[7]

Raman scattering was discovered in the beginning of the 20th century. Loudon and Fleury showed how to use it to detect magnetic excitations in the beginning of the 1960s.[8]

It was used for instance in the late 1980s to estimate the exchange in the cuprates;[9] it has also been shown to be a useful probe to investigate orbital excitations in the context of $4f$ materials where a quadrupolar ordering of orbital origin occurs.[10] More recently, the investigation of magnetic properties with this spectroscopic technique in various contexts like frustrated systems[5,6,11,12] or iron pnictides[13] has been a very active field of research.

In fact, inelastic light scattering takes advantage of the fact that the response is in essence linked to many-body physics and that the photon polarization enables one to collect valuable insights on correlated electron systems.[14,15] Following this route, we present here inelastic light scattering as a natural probe to characterize the order and the low-energy excitations in spin $S = 1$ models.

The pecularity of quantum magnets with $S > 1/2$ is that they can break SU(2) symmetry with a local order parameter that is nonmagnetic. The simplest example is provided by quadrupolar order for $S = 1$ systems, where the local order parameter is not the spin but a rank-2 tensor. This has been extensively studied in the context of the bilinear-biquadratic model defined by the Hamiltonian:

$$\mathcal{H}_{\rm eff} = J \sum_{\langle i,j \rangle} [\cos\theta(\mathbf{S}_i \cdot \mathbf{S}_j) + \sin\theta(\mathbf{S}_i \cdot \mathbf{S}_j)^2]. \qquad (1)$$

Ferro- and antiferroquadrupolar phases have been identified both on the triangular[16,17] and square[18,19] lattices for sufficiently large biquadratic interactions, and the compound $NiGa_2S_4$, where Ni^{2+} ions form a triangular lattice of spins 1, has been suggested to exhibit some kind of quadrupolar order.[16,17,20,21] Possible mechanisms to produce large biquadratic interactions include spin-lattice coupling[22] and situations with quasiorbital degeneracy.[23]

A direct observation of quadrupolar order remains a challenge, however.[16] Quadrupolar states being nonmagnetic, conventional experimental techniques such as neutron scattering are insensitive to quadrupolar order. By contrast, we show in the present work that, since light naturally couples to the charge, inelastic light scattering offers an alternative to investigate nonmagnetic states.

The paper is organized as follows: in a first section, we present the microscopic model and the derivation of the effective magnetic light-scattering operator. We discuss the form of this effective $S = 1$ operator compared to the more conventional $S = \frac{1}{2}$ case. We show that two different resonant regimes are accessible, depending on the incoming photon energy, and we discuss the different polarization geometries relevant to our problem. This leads to a section in which the expected spectra for the different phases are displayed, followed by a section devoted to a discussion concerning potential experimental checks, and by a brief conclusion.

II. EFFECTIVE LIGHT-SCATTERING OPERATOR

A. Microscopic parameters

From the point of view of purely atomic physics, spin-1 states can be achieved in the case of transition-metal ions, for instance, Ni^{2+} ($3d^8$) in a cubic environment that leads to the

standard t_{2g}-e_g splitting of the orbital d shell. The intra-atomic electron-electron interaction of the partially filled shell can then be reformulated as a Hund's coupling, which favors states maximizing the spin.

As we want to keep a very general Hubbard model, we will consider here a lattice of such sites: two degenerate orbitals at half-filling, i.e., two electrons per site, with nearest-neighbor hopping and on-site interactions that include inter- and intraorbital coupling. This two-band Hubbard model is described by the following Hamiltonian:

$$\begin{aligned}\mathcal{H}_{Hb} = &\sum_{i,j}\sum_{m,m'=a,b} t^{ij}_{m,m'} c^{\dagger}_{im\sigma} c_{jm'\sigma} + \frac{1}{2}\sum_{m,m'}\sum_{\sigma\sigma'} U_{mm'} n_{jm\sigma} n_{jm'\sigma'} \\ &+ \frac{1}{2}\sum_{m\neq m'}\sum_{\sigma\neq\sigma'} \{J_H n_{jm\sigma} n_{jm'\sigma} + J_H c^{\dagger}_{im\sigma} c_{im\sigma'} c^{\dagger}_{im'\sigma'} c_{im'\sigma} \\ &+ J_P c^{\dagger}_{im'\sigma'} c^{\dagger}_{im'\sigma} c_{im\sigma'} c_{im\sigma}\}, \end{aligned} \tag{2}$$

where i,j are the site indices, m,m' refer to the orbitals, and σ refers to the electronic spin. The hopping parameter between two neighboring orbitals is $t_{m,m'}$, the on-site Coulomb repulsion is denoted by $U_{mm'}$, J_H represents the Hund's coupling, and J_P is the pair hopping amplitude. For the sake of clarity, we restrict ourselves here to a square lattice, although the extension to other lattices is straightforward. Furthermore, we assume that the additional relations, typical of cubic symmetry, are satisfied, namely $U_{aa} = U_{bb}$, $U = U_{aa} - 2J_H$, and $J_H = 2J_P$.

In the Mott insulator regime, at half-filling and for $U_{mm'} \gg t_{m,m'}$, the electrons are localized and Hund's coupling favors triplet states on each site. The relevant degree of freedom is then a spin $S = 1$. At second order in perturbation theory, the resulting effective spin-1 Hamiltonian is the standard Heisenberg model:

$$\mathcal{H}^{(2)}_{\text{eff}} = J^{(2)}_{\text{Heis}} \sum_{\langle i,j\rangle} \mathbf{S}_i \cdot \mathbf{S}_j,$$

with

$$J^{(2)}_{\text{Heis}} = \frac{t^2_{aa} + 2t^2_{ab} + t^2_{bb}}{U + 2J_H}.$$

As in the case of $S = 1/2$ effective models for single-band Hubbard,[24,25] pushing the perturbation to fourth order leads to the emergence of additional terms such as four-site terms[26] and biquadratic interactions.

B. Derivation of the effective operator

1. General method

Inelastic light-scattering techniques like Raman are photon-in photon-out techniques where the incident photon couples to the charge. Shastry and Shraiman gave a microscopic description of the process in Ref. 27. The procedure is however given in a more pedagogical way in Ref. 6. As we follow very closely the latter, we will not explain in great detail the derivation but just sketch the main ideas. The photon-electron interaction is introduced via the Peierls substitution:

$$c_{ix\sigma} \rightarrow c_{ix\sigma} \exp\left[-i\frac{e}{\hbar c}\int_{-\infty}^{r_i} \mathbf{A}\cdot\mathbf{dl}\right],$$

where $\mathbf{A}$ is the photon vector potential.

For incoming photon wavelengths much larger than the lattice spacing, it can easily be shown that the coupling of the microscopic Hamiltonian to the photon affects only the kinetic terms and generates a current that depends on the incident ($\boldsymbol{e}_{\text{in}}$) and scattered ($\boldsymbol{e}_{\text{out}}$) polarizations. After second quantization of $\mathbf{A}$, a and $a^{\dagger}$ being respectively the photon creation and annihilation operators, the current term reads

$$\begin{aligned}\mathcal{H}_C = i\frac{e}{\hbar c}\sum_{\langle i,j\rangle}\sum_{m,m'} t^{ij}_{m,m'} c^{\dagger}_{im\sigma} c_{jm'\sigma} \\ \times \sum_{k_{\text{in}},k_{\text{out}}} \left(g_{\text{in}}\boldsymbol{e}_{\text{in}} a_{k_{\text{in}}} + g_{\text{out}}\boldsymbol{e}_{\text{out}} a^{\dagger}_{k_{\text{out}}}\right)\cdot\boldsymbol{e}_{i\rightarrow j},\end{aligned}$$

with $g_{\text{in,out}} = \sqrt{hc^2/\omega_{k_{\text{in,out}}}V}$, where V stands for the volume, and $\boldsymbol{e}_{i\rightarrow j}$ is the vector connecting site i and site j.

Hence collecting all the parts of the Hamiltonian describing the electronic system coupled to the light, we have $\mathcal{H} = \mathcal{H}_{Hb} + \mathcal{H}_C + \mathcal{H}_\gamma$, where $\mathcal{H}_\gamma$ represents the purely photonic part of the Hamiltonian.

In the limit $U \gg t$, the electrons are localized and the low-energy spectrum of the system can be described by a spin Hamiltonian. Furthermore, in the limit $|U - \omega_{\text{in}}| \lesssim t$, $\mathcal{H}_c$ can be treated as a perturbation and one can derive an effective magnetic Raman operator in the spin sector. Yet, if one is interested in having an effective operator beyond the standard limit $|U - \omega_{\text{in}}| \ll t$, one has to push the perturbation theory to fourth order. It is worth pointing out that this effective description conserves the quantum numbers of the original Hamiltonian and scattering operator: for instance, since $\mathcal{H}_{Hb}$ and $\mathcal{H}_C$ conserve the total spin, so will the effective Raman operator and thus we recover the fact that $\Delta S = 0$ for Raman excitations.

The effective scattering Hamiltonian obviously depends on the chosen polarizations of the incoming and scattered photons; to clarify the discussion, we present in Fig. 1 the different geometries we have investigated.

The scattering operator can, in general, be decomposed in two different ways: the first one involves the symmetry of this operator and the second refers to the different incoming and outgoing polarization vectors. These two decompositions are equivalent at second order, but they are different at higher order (see Ref. 28). Here, we choose to decompose the scattering operator with respect to the polarization geometries shown in Fig. 1. To stick to the most conventional notations, the top-left crossed polarization geometry of Fig. 1 will be referred to as B_{1g}, while the bottom-left geometry will be called A_{1g}.

2. Single-band case: results for $S = 1/2$

This calculation has already been done in Ref. 27. However, Ko *et al.*[6] recently pointed out some differences in some channels between the operator calculated initially and their own calculation. So, as a warm-up, we have rederived the operators for every channel. We found further differences at fourth order with respect to the initial calculation.[27,29] Defining $\mathcal{P}_\alpha \equiv \sum_r \boldsymbol{S}_r \cdot \boldsymbol{S}_{r+\alpha}$, $\mathcal{Q}_{\alpha,\beta,\delta} \equiv \sum_r (\boldsymbol{S}_r \cdot \boldsymbol{S}_{r+\alpha})(\boldsymbol{S}_{r+\beta} \cdot \boldsymbol{S}_{r+\delta})$,

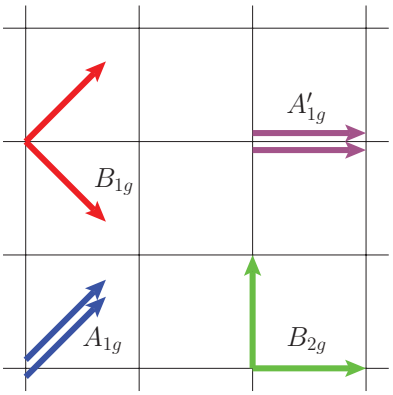

FIG. 1. (Color online) Polarization geometries for the incident and scattered photons. The present decomposition refers to the scattering sectors at second order in the derivation. Higher-order terms will mix the sectors as indicated in Table I of Ref. 27.

and $\Delta \equiv t/(U-\omega_i)$,we found

$$\mathcal{O}_{B_{1g}} = 4t\Delta\left(\tfrac{1}{2}+2\Delta^2\right)(\mathcal{P}_y-\mathcal{P}_x)-2t\Delta^3(\mathcal{P}_{2y}-\mathcal{P}_{2x}),$$

$$\begin{aligned}\mathcal{O}_{A_{1g}} &= 4t\Delta\left(\tfrac{1}{2}+6\Delta^2\right)(\mathcal{P}_y+\mathcal{P}_x)-2t\Delta^3(\mathcal{P}_{2y}+\mathcal{P}_{2x})\\ &\quad -8t\Delta^3(\mathcal{P}_{x+y}+\mathcal{P}_{x-y})+32t\Delta^3(\mathcal{Q}_{x,y,x+y}+\mathcal{Q}_{y,x,x+y}\\ &\quad -\mathcal{Q}_{x+y,x,y}),\quad \mathcal{O}_{B_{2g}}=0,\\ \mathcal{O}_{A'_{1g}} &= 4t\Delta(1+8\Delta^2)\mathcal{P}_x+16t\Delta^3\mathcal{P}_y\\ &\quad -4t\Delta^3\mathcal{P}_{2x}-8t\Delta^3(\mathcal{P}_{x+y}+\mathcal{P}_{x-y})\\ &\quad +32t\Delta^3(\mathcal{Q}_{x,y,x+y}+\mathcal{Q}_{y,x,x+y}-\mathcal{Q}_{x+y,x,y}).\end{aligned} \quad (3)$$

In Appendix A, we discuss the differences between this operator and the result of Refs. 27 and 29 after rewriting it following the symmetry-based decomposition used in this reference. To test the validity of our operators, we have also compared on small clusters the Raman spectra of the original single-band Hubbard model with those obtained with the effective operators, with the conclusion that the spectra obtained with our operators agree much better.

3. *Two-band case: results for S = 1*

The general procedure is similar to the one of the single-band case, but starting from the two-band Hamiltonian described in Sec. II A. There are two main differences between this case and the single-band case.

First, in the one-band case, the only excited states that were considered were the terms with two particles on one site, inducing a Coulomb repulsion U. These terms will still be present in the two-band case, but other terms where only the Hund's coupling is not satisfied will also be present. At fourth order, this leads to resonances at different incoming energies.

Moreover, since spin-1 live in a three-dimensional space, there are eight nontrivial Hermitian operators acting on site (instead of three in the spin-1/2 case). We thus expect new types of operator to appear, as, for example, the biquadratic coupling $(\boldsymbol{S}_i\cdot\boldsymbol{S}_j)^2$.

To express the Raman operator in this case, we take the same definition for $\mathcal{P}_\alpha$ and $\mathcal{Q}_{\alpha,\beta,\delta}$ as for spin-1/2 and we introduce in addition the operators $\mathcal{R}_\alpha \equiv \sum_r(\boldsymbol{S}_r\cdot\boldsymbol{S}_{r+\alpha})^2$ and $\mathcal{T}_{\alpha,\beta}\equiv\sum_r(\boldsymbol{S}_r\cdot\boldsymbol{S}_{r+\alpha})(\boldsymbol{S}_{r+\alpha}\cdot\boldsymbol{S}_{r+\beta})$. To fourth order in perturbation theory, the resulting operators for B_{1g} and A_{1g} read

$$\begin{aligned}\mathcal{O}_{B_{1g}} &= B_h(\mathcal{P}_x-\mathcal{P}_y)+B_b(\mathcal{R}_x-\mathcal{R}_y)\\ &\quad +B_{h2}(\mathcal{P}_{i+2x}-\mathcal{P}_{i+2y})+B_3(\mathcal{T}_{x,2x}-\mathcal{T}_{y,2y}),\\ \mathcal{O}_{A_{1g}} &= A_h(\mathcal{P}_x+\mathcal{P}_y)+A_b(\mathcal{R}_x+\mathcal{R}_y)\\ &\quad +A_d(\mathcal{P}_{x+y}+\mathcal{P}_{x-y})\\ &\quad +A_{h2}(\mathcal{P}_{2x}+\mathcal{P}_{2y})+A_3(\mathcal{T}_{x,2x}+\mathcal{T}_{y,2y})\\ &\quad +A_{3d}(\mathcal{T}_{x,x+y}+\mathcal{T}_{x,x-y}+\mathcal{T}_{y,x+y}+\mathcal{T}_{-y,x-y})\\ &\quad +A_p(\mathcal{Q}_{x,x+y,y}+\mathcal{Q}_{y,x,x+y}-\mathcal{Q}_{x+y,x,y}).\end{aligned} \quad (4)$$

The different coefficients are functions of the different parameters of the initial Hamiltonian, Eq. (2). They are given in Appendix B.

C. Relevant limits and geometries

One of the major advantages of Raman scattering lies in the possibility of using light polarization to select and characterize the excitation that one is willing to investigate. As the derivation remains very systematic, so far, we have taken care of all the different polarizations. At second order, only A_{1g} and B_{1g} geometries have nonvanishing operators. Therefore, in the rest of the paper, we will mainly focus our attention on these two cases.

In addition to the usual decomposition due to the incoming and outgoing polarizations, one should also be aware of the information that can be accessed through a suitable choice of the incoming photon energy. The Raman operators and the associated prefactors of Appendix B lead to many terms. However, since all the prefactors depend on the incoming photon energy, it is possible to adjust ω_{in} to get close to a resonance and highlight specific terms of the scattering operators.

In the limit $\hbar\omega_{\text{in}} \lesssim U+2J_H \sim U$, the second-order processes will be dominant, and the other terms can be neglected. Therefore, in this case, we can restrict ourselves to the Fleury-Loudon Raman operator:

$$\hbar\omega_{\text{in}}\sim U \Rightarrow \begin{cases}\mathcal{O}_{A1g} & \propto & \sum_r(\boldsymbol{S}_r\cdot\boldsymbol{S}_{r+x}+\boldsymbol{S}_r\cdot\boldsymbol{S}_{r+y}),\\ \mathcal{O}_{B1g} & \propto & \sum_r(\boldsymbol{S}_r\cdot\boldsymbol{S}_{r+x}-\boldsymbol{S}_r\cdot\boldsymbol{S}_{r+y}).\end{cases}$$

Another interesting limit occurs when $\hbar\omega_{\text{in}}\sim 4U$. In this case, we will favor processes where there is an intermediate state with four electrons at the same site. Such processes occur at fourth order if they involve only two sites. Moreover, as they can change the local spin by $\Delta S=2$, they have to be related to the operator $(\boldsymbol{S}_i\cdot\boldsymbol{S}_j)^2$. This explanation is confirmed by the exact coefficient of the Raman operator given in Appendix B. So, in this limit, we can consider that the Raman operator reduces to

$$\hbar\omega_{\text{in}}\sim 4U \Rightarrow \begin{cases}\mathcal{O}_{A1g} & \propto & \sum_r(\boldsymbol{S}_r\cdot\boldsymbol{S}_{r+x})^2+(\boldsymbol{S}_r\cdot\boldsymbol{S}_{r+y})^2,\\ \mathcal{O}_{B1g} & \propto & \sum_r(\boldsymbol{S}_r\cdot\boldsymbol{S}_{r+x})^2-(\boldsymbol{S}_r\cdot\boldsymbol{S}_{r+y})^2.\end{cases}$$

So, in two different limits, the Raman operator can be written in a quite simple way for the B_{1g} and the A_{1g} geometries. The next section will be devoted to an investigation of the Raman spectra calculated from these four operators in different situations.

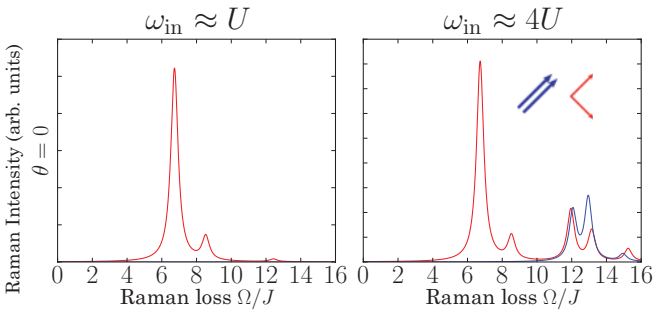

FIG. 2. (Color online) Raman spectra of the spin-1 Heisenberg model [$\theta = 0$ of the Hamiltonian of Eq. (1)] for A_{1g} and B_{1g} polarizations. The left column represents the inelastic response as a function of the energy loss for an incoming photon of energy $\hbar\omega_{\rm in} \lesssim U$, which corresponds to the Loudon-Fleury operators $\mathcal{O}_{\rm FL} \propto \sum_i [\mathbf{S}_i \cdot \mathbf{S}_{i+x} \pm \mathbf{S}_i \cdot \mathbf{S}_{i+y}]$. The right column corresponds to an incoming photon energy of $\hbar\omega_{\rm in} \lesssim 4U$, and hence to the biquadratic form of the scattering operators $\mathcal{O}_{\rm Biq} \propto \sum_i [(\mathbf{S}_i \cdot \mathbf{S}_{i+x})^2 \pm (\mathbf{S}_i \cdot \mathbf{S}_{i+y})^2]$. The spectra have been computed for a 16-site cluster.

III. RESULTS: EXPECTED SPECTRA

The goal of this section is to look at the Raman response for specific angles θ of Eq. (1). We do not mean here to give a quantitative and exhaustive analysis of the expected spectra but rather a qualitative description of them and, most importantly, of their evolution throughout the different phases. These investigations are carried out numerically. The presented spectra have been obtained with Lanczos and the continued fraction[30] for a 16-site square lattice cluster with periodic boundary conditions. This cluster has additional symmetries,[31] but this is of no consequence for our present purpose, which is to investigate the overall shape and behavior of the spectra for different phases.

The results and spectra discussed in the present section are summarized in Fig. 2 and in Fig. 3.

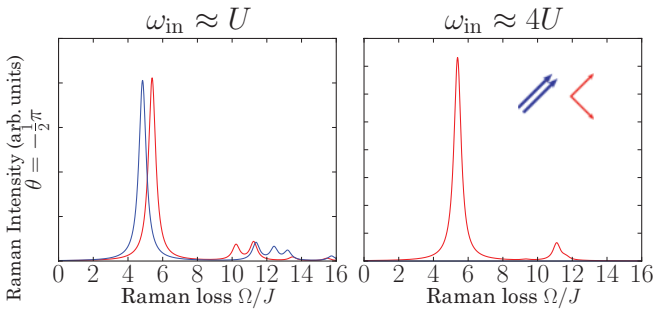

FIG. 3. (Color online) Raman spectra for a model with purely biquadratic coupling [$\theta = -\frac{\pi}{2}$ of the Hamiltonian of Eq. (1)] for A_{1g} and B_{1g} polarizations. The left column represents the inelastic response as a function of the energy loss for an incoming photon of energy $\hbar\omega_{\rm in} \lesssim U$, which corresponds to the Loudon-Fleury operators $\mathcal{O}_{\rm FL} \propto \sum_i [\mathbf{S}_i \cdot \mathbf{S}_{i+x} \pm \mathbf{S}_i \cdot \mathbf{S}_{i+y}]$. The right column corresponds to an incoming photon energy of $\hbar\omega_{\rm in} \lesssim 4U$, and hence to the biquadratic form of the scattering operators $\mathcal{O}_{\rm Biq} \propto \sum_i [(\mathbf{S}_i \cdot \mathbf{S}_{i+x})^2 \pm (\mathbf{S}_i \cdot \mathbf{S}_{i+y})^2]$. The spectra have been computed for a 16-site cluster.

A. Heisenberg AF phase

The most conventional Heisenberg antiferromagnetic phase is obviously reached for $\theta = 0$ in the Hamiltonian of Eq. (1). The Raman response in the B_{1g} geometry for the Fleury-Loudon operator exhibits a bimagnon peak, which can be understood with a standard spin-wave calculation: linear spin-wave theory leads to a peak at a Raman loss $\hbar\Omega = \hbar(\omega_{\rm in} - \omega_{\rm out}) \approx 8J$, which softens down to $\hbar\Omega \approx 7.8J$ after taking into account magnon-magnon interactions, as shown for instance by Chubukov and Frenkel[32] or Canali and Girvin.[33] This is in qualitative agreement with our numerical result. For the same polarization, the biquadratic operator gives the same response with additional peaks for higher Raman losses corresponding to multimagnon excitations.

In the A_{1g} geometry, the Fleury-Loudon operator commutes with the Heisenberg Hamiltonian and the Raman response vanishes. This is not the case for the biquadratic operator: as in the Fleury-Loudon case, the two-magnon features disappear, but the multimagnon peaks, which arise from the noncommutating part of the operator with the Hamiltonian, remain visible. It would be really interesting to check this prediction experimentally, namely that intensity shows up at larger Raman loss energy when the incoming light frequency is in the range $4U/\hbar$.

B. Ferro-quadrupolar order

For quadrupolar order, the relevant order parameter, $\mathbf{Q}$ (see Ref. 34), and its descendant observables like $\mathbf{Q} \cdot \mathbf{Q}$ can be written in terms of spin operators:

$$\mathbf{Q}_i \cdot \mathbf{Q}_j = 2(\mathbf{S}_i \cdot \mathbf{S}_j)^2 + \mathbf{S}_i \cdot \mathbf{S}_j + Cst. \qquad (5)$$

An easy point to investigate corresponds to $\theta = -\pi/2$, where the Hamiltonian reduces to its biquadratic part.

As already discussed, there are two resonant regimes: the first one for an incoming photon energy $\hbar\omega_{\rm in} \lesssim U$ leading to the bilinear Fleury-Loudon operator, and a second one for $\hbar\omega_{\rm in} \lesssim 4U$, at which the leading term of the scattering operator is proportional to $(\mathbf{S}_i \cdot \mathbf{S}_j)^2$. Since in Eq. (5) both bilinear and biquadratic couplings appear in the quadrupole-quadrupole observable, both resonant regimes offer the possibility to investigate quadrupolar order.

Concerning the physics occurring at $\hbar\omega_{\rm in} \lesssim U$, the Fleury-Loudon scattering Hamiltonian is expected to give access to quadrupolar excitations, and this turns out to be the case: the Raman response exhibits a marked peak for a Raman loss of $\hbar\Omega \approx 5J$, which can be understood as coming from a pair of quadrupolar excitations. Indeed, a flavor-wave[34,35] calculation gives the dispersion of the quadrupolar excitations across the Brillouin zone, as displayed in Fig. 4, with a $2J$ excitation at $(\pi,0)$, leading to a peak close to a Raman loss of $4J$. This prediction corresponds to the excitation of two noninteracting quadrupolar excitations. However, this simple picture does not take into account particle-particle interactions, which in the present case appear to shift the peak position at higher energy. At first glance, it is not obvious that the Loudon-Fleury scattering operator offers the possibility to investigate quadrupolar excitations, since this scattering resonance is mostly known to highlight the bimagnon peak. Yet, in contrast to the conventional magnetic scattering, the two

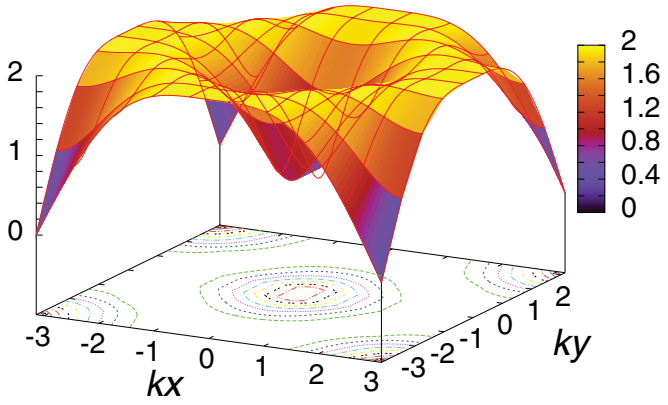

FIG. 4. (Color online) Flavor-wave dispersion for a ferro-quadrupolar order corresponding to $\theta = -\pi/2$ in Eq. (1).

scattering geometries, A_{1g} and B_{1g}, have comparable spectra, as none of the operator commutes with the Hamiltonian. The similarity of the two spectra for the two polarization geometries seems to be a signature of a ferro-quadrupolar phase.

The second resonance, for an incoming photon energy of $\hbar\omega_{\rm in} \lesssim 4U$, is associated to a scattering operator with biquadratic spin terms. As quadrupolar ordered phases are a ground state of the Hamiltonian when $(\mathbf{S}_i \cdot \mathbf{S}_j)^2$ dominates, one expects that the effective Raman operator for $\hbar\omega_{\rm in} \lesssim 4U$ probes directly quadrupolar excitations. Indeed, this is confirmed by our calculations and the obtained results can be explained in a straightforward manner. For the A_{1g} geometry, the Raman operator commutes with the Hamiltonian, hence the response vanishes. One should note, however, that for real systems many terms appear in the scattering operator and longer-range terms in the Hamiltonian should also be considered; all these facts combine to give a finite Raman response even in this geometry. Yet, exactly as for conventional magnetic Raman scattering, the amplitude of the response should be much stronger for B_{1g} polarizations, as shown in Fig. 2. One recovers the quadrupolar excitation at $\hbar\Omega \approx 5J$.

IV. DISCUSSION

As summarized in Figs. 2 and 3, the signal corresponding to a Néel ordered and a ferro-quadrupolar phase are qualitatively different. Hence Raman scattering offers the opportunity to detect quadrupolar ordering in a relatively straightforward manner. The systematic is rather simple: one should analyze the Raman spectra obtained for two scattering geometries (parallel and crossed polarizations) as presented here and tune the incoming photon energy, this last step being of course the most crucial one as it enables one to switch from the standard Loudon-Fleury limit to the biquadratic form of the scattering operator. This is one of the main messages of the paper: the microscopic derivation of an effective magnetic scattering operator for $S = \frac{1}{2}$ systems leads to one resonance at $\hbar\omega_{\rm in} \lesssim U$, since there is only one possible intermediate state. This situation is no longer valid for $S = 1$ compounds; as a spin-1 is formed by a system of two electrons per site strongly coupled *via* Hund's rule, different intermediate states can be accessed: one with three electrons at one site, leading to the usual resonance at $\hbar\omega_{\rm in} \lesssim U$ and another one with four electrons at one site leading to a second resonance at $\hbar\omega_{\rm in} \lesssim 4U$. Of course, many other intermediate states are possible, however, at second order, the only possibility is to have three electrons at one site; therefore, the Loudon-Fleury term will dominate and, at fourth order, biquadratic terms are only appearing along with intermediate states having quadruple occupancies.

However, going from the first resonant regime ($\hbar\omega_{\rm in} \lesssim U$) to the second one ($\hbar\omega_{\rm in} \lesssim 4U$) requires an adequacy between the materials and the available light source. Indeed, having a handle on the in and out polarizations remains much easier for visible light and, if U is too large, one would end up with incoming photons in the UV region of the light spectrum. A promising route might be to try organic systems, in which all interactions, including U, are smaller than in oxides.

Turning to the specific case of the ferro-quadrupolar phase, the experimental investigation would require two steps: (i) for an incoming photon energy of $\hbar\omega_{\rm in} \lesssim U$, one should start with a geometry corresponding to the A_{1g} polarization and observe a spectrum with a peak at about $\hbar\Omega \approx 5J$. By keeping the same photon energy and slowly rotating the outgoing polarization until getting to the B_{1g} polarization, one should not observe much variation, but a small hardening of the main peak. (ii) The second step consists of tuning the incoming photon energy to $\hbar\omega_{\rm in} \lesssim 4U$ and, to collect the spectra for the different polarizations from B_{1g} to A_{1g}, the Raman response should this time exhibit strong modifications: going from a marked peak to much broader features. In principle, performing the experiment within the Loudon-Fleury limit should be sufficient. However, if one does not know precisely the value of J in the considered compound, this two-step procedure allows a clear identification of the ferro-quadrupolar order. Precise calculations for the specific compound would also give information about J after fitting the data. Also, and from a more fundamental perspective, one should notice that the second resonance regime should exist even in the case of a standard Heisenberg phase. In this situation, the Raman spectra should exhibit not only a bimagnon peak, but also more spectral weight at higher energy loss.

V. CONCLUSION

In the present paper, we have derived a general effective inelastic light-scattering operator for spin-1. We have shown that this operator offers two different resonant regimes depending on the choice of the incoming photon energy. On the basis of calculated spectra, obtained by exact diagonalization of finite clusters, we have shown that the different phases of interest (Néel and ferro-quadrupolar) exhibit characteristic fingerprints that allow a clear identification of each type of ordering. This work, for the square lattice, illustrates the potential of the Raman scattering technique as a probe for characterizing quadrupolar order; one of the best candidates for such a phase remains $NiGa_2S_4$, where the spin $S = 1$ located on the Ni^{2+} ions form a triangular lattice. It is clear that a direct application for this compound is not entirely possible, as it requires another derivation and a suitable decomposition of the scattering channels, which is left for further investigation.

ACKNOWLEDGMENTS

We would like to thank H. M. Rønnow and T. A. Tóth for useful discussions. F.V. would like to thank EPFL and the CTMC group for hospitality. MaNEP and SNF are acknowledged for financial support.

APPENDIX A: COMPARISON OF EFFECTIVE RAMAN OPERATORS

In this Appendix, we aim at comparing an effective magnetic Raman scattering operator in the Mott insulating state for a spin $S = \frac{1}{2}$ model to the original Raman current operator that is associated to the Hubbard model. We present here a comparison for the Hubbard model on an $(4 \times 2 = 8)$-site ladder for B_{1g} polarization as well as for a six-site chain. The effective scattering operator derived in the present paper shows some differences compared to Shastry and Shraiman's; we also provide graphs to compare our results to theirs.

In order to stick to Shastry and Shraiman's original notations of Ref. 27, we recall their results for the reader:

$$\begin{aligned}\mathcal{O}_s &= 2t\Delta(\mathcal{P}_y + \mathcal{P}_x) + 8t\Delta^3(\mathcal{P}_{2x} + \mathcal{P}_{2y} + \mathcal{P}_{x+y} + \mathcal{P}_{x-y}) \\ &\quad + 32t\Delta^3(\mathcal{Q}_{x,y,x+y} + \mathcal{Q}_{y,x,x+y} - \mathcal{Q}_{x+y,x,y}),\\ \mathcal{O}_d &= 4t\Delta\left[\tfrac{1}{2} - 4\Delta^2\right](\mathcal{P}_y - \mathcal{P}_x) + 8t\Delta^3(\mathcal{P}_{2y} - \mathcal{P}_{2x}),\\ \mathcal{O}_o &= 64t\Delta^3 \sum_r i\epsilon_{\mu,\mu'}\mathbf{S}_{\mathbf{r}} \cdot (\mathbf{S}_{\mathbf{r}+\mu} \times \mathbf{S}_{\mathbf{r}+\mu'}),\\ \mathcal{O}_e &= -16t\Delta^3(\mathcal{P}_{x+y} + \mathcal{P}_{y-x}). \end{aligned} \tag{A1}$$

While our derivation gives

$$\begin{aligned}\mathcal{O}_s &= (2t\Delta + 24t\Delta^3)(\mathcal{P}_y + \mathcal{P}_x) - 2t\Delta^3(\mathcal{P}_{2x} + \mathcal{P}_{2y}) \\ &\quad - 8t\Delta^3(\mathcal{P}_{x+y} + \mathcal{P}_{x-y}) \\ &\quad + 32t\Delta^3(\mathcal{Q}_{x,y,x+y} + \mathcal{Q}_{y,x,x+y} - \mathcal{Q}_{x+y,x,y}),\\ \mathcal{O}_d &= 4t\Delta\left[\tfrac{1}{2} + 2\Delta^2\right](\mathcal{P}_y - \mathcal{P}_x) - 2t\Delta^3(\mathcal{P}_{2y} - \mathcal{P}_{2x}),\\ \mathcal{O}_o &= 0, \quad \mathcal{O}_e = 0. \end{aligned} \tag{A2}$$

Ko *et al.*[6] already noticed that there is no chiral term appearing in $\mathcal{O}_o$, unlike in Shastry and Shraiman's derivation. To check our derivation, we perform a numerical analysis on finite clusters. The quantities we compare are the height of a most prominent peak in the exact model and the height of the same peak in the effective model at second and fourth order. We performed this analysis on two different clusters.

(1) A $(2 \times 4 = 8)$-site cluster with open boundary conditions. This choice is motivated by the fact that it is the smallest cluster where some bounds have the correct prefactor in the x direction (for smaller clusters, some fourth-order renormalization factors will not be present in the term $\boldsymbol{S}_i \cdot \boldsymbol{S}_{i+x}$), while periodic boundary conditions would lead to the renormalization of some terms with respect to the infinite case coming from processes where a doublon goes through the four sites of one leg. The results for this cluster are presented in Fig. 5.

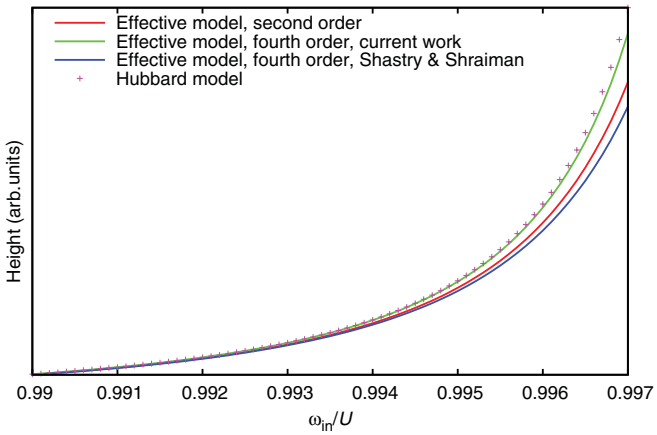

FIG. 5. (Color online) Comparison of the height of the main Raman peak for a fixed Raman loss as a function of the incoming photon energy for different models for a (2×4)-site ladder with open boundary conditions. The hopping amplitude has been set to $t = \frac{U}{2000}$, so that $t \ll U$ and $J = \frac{4t^2}{U} = \frac{U}{10^6}$.

(2) A six-site chain with periodic boundary conditions. This cluster is very useful to check the prefactor of $\boldsymbol{S}_i \cdot \boldsymbol{S}_{i+2x}$. As the term $\boldsymbol{S}_i \cdot \boldsymbol{S}_{i+x}$ commutes with the Hamiltonian on this cluster, only the $\boldsymbol{S}_i \cdot \boldsymbol{S}_{i+2x}$ term contributes to the scattering amplitude; thus we can check very precisely the coefficient. Here, it is not possible for a doublon to travel through the entire system at fourth order, and therefore we can choose periodic boundary conditions. The results for this cluster are presented in Fig. 6.

As can be seen in these figures, in both cases the spectrum derived from our effective Raman operator agrees very well with that calculated directly with the original Hubbard model, while the effective operator of Shastry and Shraiman leads to significant differences beyond the second order.

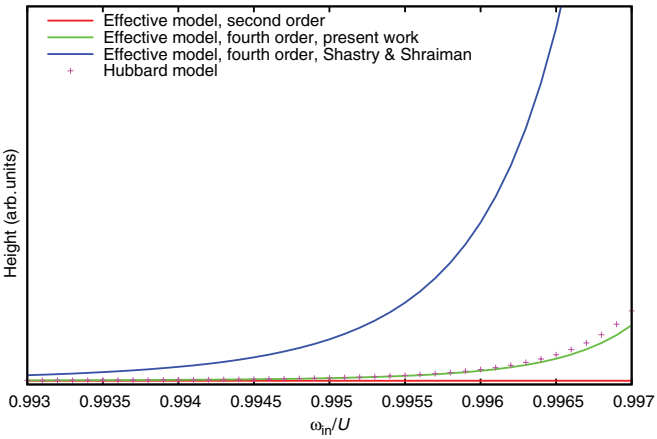

FIG. 6. (Color online) Same as Fig. 5 for a six-site chain with periodic boundary conditions.

APPENDIX B: COEFFICIENTS OF THE EFFECTIVE SPIN-1 RAMAN OPERATOR

In this Appendix, we list the expression of the prefactors of the effective spin-1 Raman operator defined in Eq. (4). The terms enclosed in a square box are those that dominate at the two resonances:

$$
\begin{aligned}
B_h &= \boxed{\frac{t_{aa}^2+2t_{ab}^2+t_{bb}^2}{2(2J_H+U-\omega_{\rm in})}}+\frac{2t_1^4+8t_2^4+4t_4^4+2t_{ab}^4}{(2J_H+U-\omega_{\rm in})^3}\\
&\quad+\frac{2(t_1^4-2t_4^4+t_{ab}^4)}{(2J_H+U-\omega_{\rm in})^2(4J_H+U-\omega_{\rm in})}-\frac{4t_4^4}{(2J_H+U-\omega_{\rm in})^2(5J_H-2J_P+U-\omega_{\rm in})}\\
&\quad+\frac{2\left(t_{2p}^4+t_{ab}^4\right)}{(2J_H+U-\omega_{\rm in})^2(5J_H-2J_P+U-\omega_{\rm in})}+\frac{2(4t_2^4+t_{2p}^4+2t_4^4+t_{ab}^4)}{(2J_H+U-\omega_{\rm in})^2(5J_H+2J_P+U-\omega_{\rm in})},\\
B_{h2} &= \frac{-2t_1^4-8t_2^4-4t_4^4-2t_{ab}^4}{(2J_H+U-\omega_{\rm in})^3}+\frac{t_1^4-2t_4^4+t_{ab}^4}{(2J_H+U-\omega_{\rm in})^2(4J_H+U-\omega_{\rm in})}\\
&\quad+\frac{t_{2p}^4-2t_4^4+t_{ab}^4}{(2J_H+U-\omega_{\rm in})^2(5J_H-2J_P+U-\omega_{\rm in})}+\frac{4t_2^4+t_{2p}^4+2t_4^4+t_{ab}^4}{(2J_H+U-\omega_{\rm in})^2(5J_H+2J_P+U-\omega_{\rm in})},\\
B_b &= \boxed{-\frac{4\left(t_{2p}^4-2t_4^4+t_{ab}^4\right)}{(2J_H+U-\omega_{\rm in})^2(4U-\omega_{\rm in})}},\\
B_3 &= \frac{t_1^4+4t_2^4+2t_4^4+t_{ab}^4}{(2J_H+U-\omega_{\rm in})^3}+\frac{-t_1^4+2t_4^4-t_{ab}^4}{(2J_H+U-\omega_{\rm in})^2(4J_H+U-\omega_{\rm in})}\\
&\quad+\frac{-t_{2p}^4+2t_4^4-t_{ab}^4}{(2J_H+U-\omega_{\rm in})^2(5J_H-2J_P+U-\omega_{\rm in})}+\frac{-4t_2^4-t_{2p}^4-2t_4^4-t_{ab}^4}{(2J_H+U-\omega_{\rm in})^2(5J_H+2J_P+U-\omega_{\rm in})},
\end{aligned}
$$

where the parameters t_1, t_2, t_{2p}, t_4 are defined in terms of the original microscopic hopping parameters by

$$
t_1^4=\tfrac{1}{2}(t_{aa}^4+t_{bb}^4),\quad t_2^4=\tfrac{1}{2}(t_{aa}^2t_{ab}^2+t_{ab}^2t_{bb}^2),\quad t_{2p}^4=t_{aa}^2t_{bb}^2,\quad t_4^4=t_{aa}t_{ab}^2t_{bb},
$$

$$
\begin{aligned}
A_h &= \boxed{\frac{t_{aa}^2+2t_{ab}^2+t_{bb}^2}{2(2J_H+U-\omega_{\rm in})}}+\frac{4t_1^4+16t_2^4+8t_4^4+4t_{ab}^4}{(2J_H+U-\omega_{\rm in})^3}+\frac{4\left(t_1^4-2t_4^4+t_{ab}^4\right)}{(2J_H+U-\omega_{\rm in})^2(4J_H+U-\omega_{\rm in})}\\
&\quad-\frac{8t_4^4}{(2J_H+U-\omega_{\rm in})^2(5J_H-2J_P+U-\omega_{\rm in})}+\frac{4\left(t_{2p}^4+t_{ab}^4\right)}{(2J_H+U-\omega_{\rm in})^2(5J_H-2J_P+U-\omega_{\rm in})}\\
&\quad+\frac{4\left(4t_2^4+t_{2p}^4+2t_4^4+t_{ab}^4\right)}{(2J_H+U-\omega_{\rm in})^2(5J_H+2J_P+U-\omega_{\rm in})}+\frac{4\left(t_{2p}^4-2t_4^4+t_{ab}^4\right)}{(2J_H+U-\omega_{\rm in})^2(2J_H+3U-\omega_{\rm in})},\\
A_{h2} &= \frac{-2t_1^4-8t_2^4-4t_4^4-2t_{ab}^4}{(2J_H+U-\omega_{\rm in})^3}+\frac{t_1^4-2t_4^4+t_{ab}^4}{(2J_H+U-\omega_{\rm in})^2(4J_H+U-\omega_{\rm in})}\\
&\quad+\frac{t_{2p}^4-2t_4^4+t_{ab}^4}{(2J_H+U-\omega_{\rm in})^2(5J_H-2J_P+U-\omega_{\rm in})}+\frac{4t_2^4+t_{2p}^4+2t_4^4+t_{ab}^4}{(2J_H+U-\omega_{\rm in})^2(5J_H+2J_P+U-\omega_{\rm in})},\\
A_b &= \boxed{-\frac{4\left(t_{2p}^4-2t_4^4+t_{ab}^4\right)}{(2J_H+U-\omega_{\rm in})^2(4U-\omega_{\rm in})}},\quad A_3=\frac{t_1^4+4t_2^4+2t_4^4+t_{ab}^4}{(2J_H+U-\omega_{\rm in})^3}+\frac{-t_1^4+2t_4^4-t_{ab}^4}{(2J_H+U-\omega_{\rm in})^2(4J_H+U-\omega_{\rm in})}\\
&\quad+\frac{-t_{2p}^4+2t_4^4-t_{ab}^4}{(2J_H+U-\omega_{\rm in})^2(5J_H-2J_P+U-\omega_{\rm in})}+\frac{-4t_2^4-t_{2p}^4-2t_4^4-t_{ab}^4}{(2J_H+U-\omega_{\rm in})^2(5J_H+2J_P+U-\omega_{\rm in})},
\end{aligned}
$$

$$A_d = \frac{-8t_1^4 - 32t_2^4 - 16t_4^4 - 8t_{ab}^4}{(2J_H + U - \omega_{\rm in})^3} + \frac{2(t_1^4 - 2t_4^4 + t_{ab}^4)}{(2J_H + U - \omega_{\rm in})^2(4J_H + U - \omega_{\rm in})}$$
$$- \frac{4t_4^4}{(2J_H + U - \omega_{\rm in})^2(5J_H - 2J_P + U - \omega_{\rm in})} + \frac{2(t_{2p}^4 + t_{ab}^4)}{(2J_H + U - \omega_{\rm in})^2(5J_H - 2J_P + U - \omega_{\rm in})}$$
$$+ \frac{2(4t_2^4 + t_{2p}^4 + 2t_4^4 + t_{ab}^4)}{(2J_H + U - \omega_{\rm in})^2(5J_H + 2J_P + U - \omega_{\rm in})},$$

$$A_p = -\frac{2(2t_1^4 + 8t_2^4 + 4t_4^4 + 2t_{ab}^4)}{(2J_H + U - \omega_{\rm in})^3}, \quad A_{3d} = \frac{t_1^4 + 4t_2^4 + 2t_4^4 + t_{ab}^4}{(2J_H + U - \omega_{\rm in})^3} + \frac{-t_1^4 + 2t_4^4 - t_{ab}^4}{(2J_H + U - \omega_{\rm in})^2(4J_H + U - \omega_{\rm in})}$$
$$+ \frac{-t_{2p}^4 + 2t_4^4 - t_{ab}^4}{(2J_H + U - \omega_{\rm in})^2(5J_H - 2J_P + U - \omega_{\rm in})} + \frac{-4t_2^4 - t_{2p}^4 - 2t_4^4 - t_{ab}^4}{(2J_H + U - \omega_{\rm in})^2(5J_H + 2J_P + U - \omega_{\rm in})}.$$

[1] P. W. Anderson, Science **235**, 1196 (1987).
[2] F. Mila, Phys. Rev. Lett. **81**, 2356 (1998).
[3] D. S. Rokhsar and S. A. Kivelson, Phys. Rev. Lett. **61**, 2376 (1988).
[4] R. Moessner and S. L. Sondhi, Phys. Rev. Lett. **86**, 1881 (2001).
[5] O. Cépas, J. O. Haerter, and C. Lhuillier, Phys. Rev. B **77**, 172406 (2008).
[6] W.-H. Ko, Z.-X. Liu, T.-K. Ng, and P. A. Lee, Phys. Rev. B **81**, 024414 (2010).
[7] D. Wulferding, P. Lemmens, P. Scheib, J. Roder, P. Mendels, S. Chu, T. Han, and Y. S. Lee, Phys. Rev. B **82**, 144412 (2010).
[8] P. A. Fleury and R. Loudon, Phys. Rev. **166**, 514 (1968).
[9] K. B. Lyons, P. A. Fleury, J. P. Remeika, A. S. Cooper, and T. J. Negran, Phys. Rev. B **37**, 2353 (1988).
[10] T. Nagao and J.-i. Igarashi, J. Phys. Soc. Jpn. **71**, 618 (2002).
[11] N. Perkins and W. Brenig, Phys. Rev. B **77**, 174412 (2008).
[12] F. Vernay, T. P. Devereaux, and M. J. P. Gingras, J. Phys. Condens. Matter **19**, 145243 (2007).
[13] C.-C. Chen, C. J. Jia, A. F. Kemper, R. R. P. Singh, and T. P. Devereaux, Phys. Rev. Lett. **106**, 067002 (2011).
[14] T. P. Devereaux and R. Hackl, Rev. Mod. Phys. **79**, 175 (2007).
[15] J. Deisenhofer and P. Lemmens, in *Introduction to Highly Frustrated Magnetism*, Vol. 164 of Springer Series in Solid-State Sciences, edited by C. Lacroix, P. Mendels, and F. Mila (Springer, New York, 2011), pp. 107–128.
[16] H. Tsunetsugu and M. Arikawa, J. Phys. Soc. Jpn. **75**, 083701 (2006).
[17] A. Läuchli, F. Mila, and K. Penc, Phys. Rev. Lett. **97**, 087205 (2006).
[18] K. Harada and N. Kawashima, Phys. Rev. B **65**, 052403 (2002).
[19] T. A. Tóth, A. M. Läuchli, F. Mila, and K. Penc, Phys. Rev. Lett. **105**, 265301 (2010); (unpublished).
[20] S. Nakatsuji *et al.*, Science **309**, 1697 (2005).
[21] S. Nakatsuji *et al.*, J. Phys. Condens. Matter **19**, 145232 (2007).
[22] C. Kittel, Phys. Rev. **120**, 335 (1960).
[23] F. Mila and F.-C. Zhang, Eur. Phys. J. B **16**, 7 (2000).
[24] A. H. MacDonald, S. M. Girvin, and D. Yoshioka, Phys. Rev. B **37**, 9753 (1988).
[25] J.-Y. P. Delannoy, M. J. P. Gingras, P. C. W. Holdsworth, and A.-M. S. Tremblay, Phys. Rev. B **72**, 115114 (2005).
[26] R. Bastardis, N. Guihéry, and C. de Graaf, Phys. Rev. B **76**, 132412 (2007).
[27] B. S. Shastry and B. I. Shraiman, Phys. Rev. Lett. **65**, 1068 (1990).
[28] J. K. Freericks and T. P. Devereaux, Phys. Rev. B **64**, 125110 (2001).
[29] B. S. Shastry and B. I. Shraiman, Int. J. Mod. Phys. B **5**, 365 (1991).
[30] E. Dagotto, Rev. Mod. Phys. **66**, 763 (1994).
[31] A. W. Sandvik, S. Capponi, D. Poilblanc, and E. Dagotto, Phys. Rev. B **57**, 8478 (1998).
[32] A. V. Chubukov and D. M. Frenkel, Phys. Rev. B **52**, 9760 (1995).
[33] C. M. Canali and S. M. Girvin, Phys. Rev. B **45**, 7127 (1992).
[34] K. Penc and A. M. Läuchli, in *Introduction to Highly Frustrated Magnetism*, Vol. 164 of Springer Series in Solid-State Sciences, edited by C. Lacroix, P. Mendels, and F. Mila (Springer, New York, 2011), pp. 331–360.
[35] N. Papanicolaou, Nucl. Phys. B **305**, 367 (1988).